Optical Excitation and Trapping of ^{81}Kr

J. S. Wang, F. Ritterbusch,[*] X.-Z. Dong, C. Gao, H. Li, W. Jiang, S.-Y. Liu, Z.-T. Lu,[†]
W.-H. Wang, G.-M. Yang, Y.-S. Zhang, and Z.-Y. Zhang

Hefei National Laboratory for Physical Sciences at the Microscale,
CAS Center for Excellence in Quantum Information and Quantum Physics,
University of Science and Technology of China, 96 Jinzhai Road, Hefei 230026, China

We have realized optical excitation, trapping, and detection of the radioisotope ^{81}Kr with an isotopic abundance of 0.9 ppt. The 124 nm light needed for the production of metastable atoms is generated by a resonant discharge lamp. Photon transport through the optically thick krypton gas inside the lamp is simulated and optimized to enhance both brightness and resonance. We achieve a state-of-the-art ^{81}Kr loading rate of 1800 atoms/h, which can be further scaled up by adding more lamps. The all-optical approach overcomes the limitations on precision and sample size of radiokrypton dating, enabling new applications in the earth sciences, particularly for dating of polar ice cores.

Introduction.—^{81}Kr ($t_{1/2} = 229$ ka) is the ideal isotope for radiometric dating of water and ice in the age range from 30 000 years to over 1×10^6 years [1,2]. Atom trap trace analysis (ATTA) [3], an analytical method that detects single atoms via their fluorescence in a magneto-optical trap (MOT), has overcome the difficulties of detecting this isotope at the extremely low isotopic abundance levels of 10^{-14}–10^{-12} in the environment, enabling a wide range of applications in the earth sciences [2,4]. The required sample size for ^{81}Kr analysis is 1 μL (at standard temperature and pressure) of krypton, which can be extracted from 10–20 kg of water or ice [5,6]. The upper age reach is 1.3×10^6 years at which the ^{81}Kr isotopic abundance drops to $\sim 2\%$ of the modern level [6]. However, the sample size requirement is still too large and the upper age reach still does not go back far enough for ^{81}Kr to unveil its full potential, especially for major questions in paleoclimatology such as the mid-pleistocene transition [7,8], the Greenland ice sheet stability [9,10], or the stability of ice caps on the Tibetan plateau [11–13].

Laser cooling and trapping of krypton atoms in the ground level is not feasible due to the lack of suitable lasers at the required VUV wavelength. Instead, the krypton atoms first need to be transferred to the metastable level $1s_5$ where the $1s_5 - 2p_9$ cycling transition at 811 nm can then be employed (Fig. 1). The level $1s_5$ is ~ 10 eV above the ground level and, in operational ATTA instruments, is populated by electron-impact excitation in a discharge. However, the electron-atom collisions also destroy metastable atoms via deexcitation and ionization [14–16], leading to a metastable population fraction of only 10^{-4}–10^{-3}. Meanwhile, krypton ions are implanted into the surfaces of the vacuum system leading to sample loss, and previously embedded krypton is sputtered out causing

cross-sample contamination. These are currently the main limitations for reducing the sample size as well as extending the age range of ^{81}Kr dating.

These limitations of the discharge excitation can be overcome by optically exciting the krypton atoms from the ground to the metastable level. One realization is via off-resonant two-photon excitation to the level $2p_6$, requiring a laser at 215 nm, followed by a spontaneous decay to $1s_5$. This mechanism has recently been demonstrated in a spectroscopy cell using a pulsed optical parametric oscillator laser [17]. Metastable production efficiencies up to 2% per pulse (2 mJ per 5 ns long pulses, 10 Hz repetition rate) were achieved in the focus region of 0.1 mm across. For this scheme to be applicable in a practical ATTA system, laser powers would have to be higher by several orders of magnitude. Another way to optically excite the
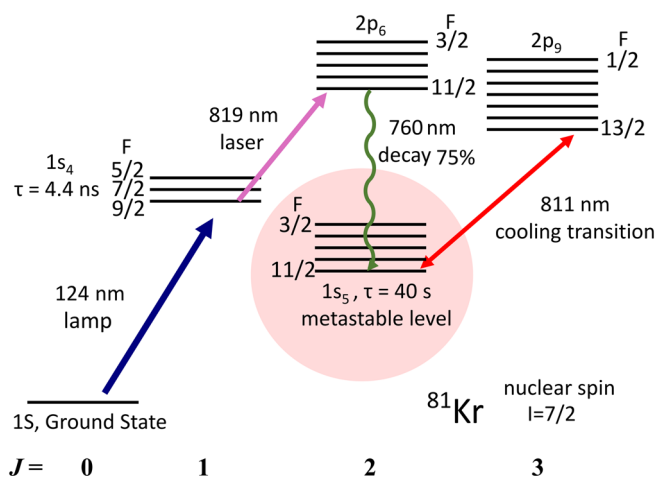

FIG. 1. Optical excitation schematic for ^{81}Kr.

krypton atoms is by resonant two-photon excitation via the 124 nm and 819 nm transition (Fig. 1). Light at 124 nm can be generated by four-wave-mixing in a mercury cell [18,19] or by a free electron laser [20]. At least 1 mW of time-averaged power within the resonant linewidth of ~3 GHz would be needed for this excitation scheme.

Instead of relying on a VUV laser, the 124 nm photons can also be generated by a krypton discharge lamp with the commercial krypton in the lamp being strictly separated from the sample krypton in the measurement chamber. The production of metastable krypton using this approach was demonstrated both in a cell [21,22] and a beam [23]. It was also used to demonstrate laser trapping of the abundant isotopes of krypton [24]. However, the lack of a lamp with sufficiently high VUV intensity has so far precluded the implementation of optical excitation in an ATTA system for [81]Kr detection. A particular difficulty is self-absorption of the 124 nm photons in the lamp. According to previous analyses based on Lambert-Beer type calculations, self-absorption leads to a reduced intensity as well as a reversed line profile [21,25–27]. With Monte Carlo simulations of the photon transport in the lamp, we find that the absorbed photons are not lost but that through a multiple scattering process their frequencies are changed. This finding is confirmed by measurements, which agree with simulation results for the VUV output spectrum and the metastable excitation efficiency. The discharge lamp optimized based on these findings has allowed us to realize all-optical atom trap trace analysis of [81]Kr at the natural abundance level.

Experimental setup.—For trapping and detection of individual [81]Kr atoms we have developed an ATTA system similar to that described in Refs. [4,28] but customized to the deployment of optical excitation. The single [81]Kr atoms are detected via their 811 nm fluorescence in the MOT. The loading rate of an abundant isotope is determined by first clearing the MOT with the quenching transition and then measuring the initial linear part of the rising slope of the MOT fluorescence [29]. The krypton discharge lamp is installed at the outlet of the source tube as illustrated in Fig. 2. The 819 nm laser beam is directed along the axis of the atom beam to enable a long interaction region illuminated by the 124 nm light from the lamp. The discharge lamp is powered by a rf coil and designed in flow configuration, so that contaminants produced in the discharge are continuously carried away. The VUV photons exit the lamp through a magnesium-fluoride (MgF_2) window, which has a transmission of about 70% at 124 nm. A quartz tube (5 mm inner diameter) with a hole at the bottom (2 mm) enables a strong pressure gradient between the upper discharge part and the ~2 mm gap right on top of the MgF_2 window. This design has proven to be important for maintaining a strong discharge while, close to the window, the number of scattering events are minimized (see following section). A quartz liner prevents the discharge from impinging on the metal support, which would
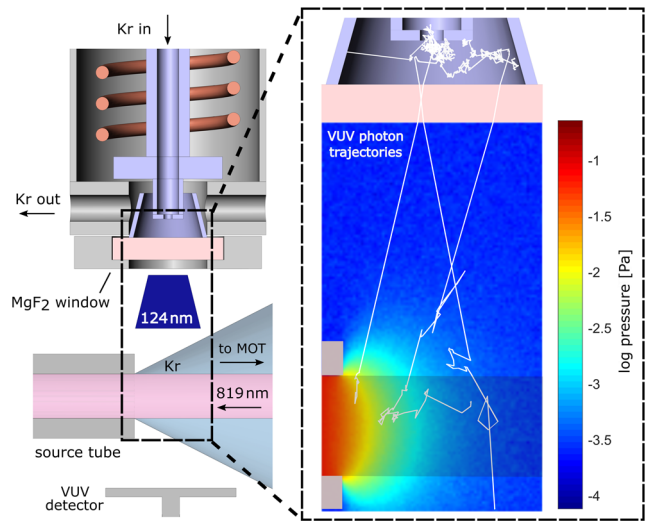

FIG. 2. Optical excitation implemented on an ATTA setup for [81]Kr detection. The 124 nm light is generated with a discharge lamp oriented perpendicular to the atomic beam. The 819 nm light is directed counterpropagating to the atomic beam. A VUV detector below the lamp measures the VUV intensity. On the right side, a close-up view of the excitation region is shown including the pressure distribution at the outlet of the source tube. The 819 nm beam is indicated by the shaded area. Typical 124 nm-photon trajectories, generated by a Monte Carlo simulation, are shown in white.

lead to deposition of contaminants on the MgF_2 window. The quartz body as well as the MgF_2 window are sealed with resilient aluminum gaskets. The VUV intensity of the lamp is measured via the photoelectric emission from a biased stainless steel plate below the lamp. The measured photon flux on the detector is typically ~2×10^{15} photons/s, translating to a photon flux density in forward direction of ~3×10^{16} photons/s/sr, comparable to that reported in previous works [21,30]. The key development in this work has been on improving the resonance without compromising irradiance.

Simulated frequency spectrum of the lamp.—Due to scattering processes in the discharge lamp, the output spectrum is strongly altered from the initial Doppler distribution [31,32]. In order to understand the process and its dependencies, we have performed Monte Carlo simulations of the VUV photon scattering in the lamp and the resulting frequency shifts. Photons are generated with a random frequency according to the Doppler distribution at the outlet of the quartz tube. The trajectories of the photons through the lamp are traced until they either escape through the MgF_2 window or hit the quartz wall. Typical 124 nm-photon trajectories in the lamp (Fig. 2) show that the photons undergo a large number of scattering events before they obtain a sufficiently large detuning to cross the krypton gas and leave the lamp. The simulated emission spectra are shown in Fig. 3. Interestingly, the total VUV intensity does not change significantly for different lamp
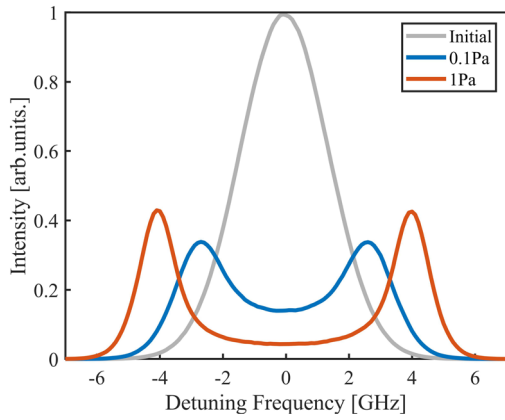
FIG. 3. Simulated emission spectra of the lamp at different krypton pressures experimentally relevant to this work. The initial distribution is a Doppler-broadened spectrum at room temperature.

pressures. For 0.1 Pa, it is almost the same as for 1 Pa, amounting to about half of the initial intensity (gray line in Fig. 3). This is contrary to the calculation based on Lambert-Beer's law, which yields a decrease in the VUV intensity by several orders of magnitude as the pressure increases. The simulation shows that at a higher lamp pressure the VUV intensity is not decreasing but that the output spectrum is becoming off-resonant. Consequently, a lamp design that can maintain a high irradiance at a low krypton pressure close to the MgF_2 window, as realized in this work, is needed.

The simulation continues to follow the 124 nm-photons as they exit the lamp and are scattered in the atomic beam leading to the production of metastable krypton atoms. The pressure distribution at the exit of the source tube is

obtained using a test-particle Monte-Carlo simulator for vacuum systems [33]. The resulting pressure distribution is shown in Fig. 2 together with typical 124 nm-photon trajectories. The 124 nm photons travel relatively undisturbed from the lamp to the exit of the source tube due to the low pressure along the path and the large detuning when leaving the lamp. Upon entering the higher pressure region at the exit of the source tube, the scattering probability increases drastically. After the first scattering event in the higher pressure region, the 124 nm photons are likely to become more resonant and will therefore be scattered until combining with an 819 nm photon to produce a metastable krypton atom. A similar result has previously been obtained by a Monte Carlo study in a krypton cell [21], including effects of photon scattering and energy redistribution.

Results and discussion.—The MOT loading rate of the abundant ^{83}Kr (11.5% isotopic abundance) is measured while the frequency of the 819 nm laser is scanned across the resonances of the hyperfine manifolds of the $1s_4 - 2p_6$ transition [Fig. 4(a)]. The highest loading rate occurs at the overlap of the transitions $F = 7/2 \rightarrow 9/2$ and $F = 9/2 \rightarrow 11/2$. The $F = 11/2 \rightarrow 13/2$ transition is similarly high as expected from the transition strength [34]. In order to address not only one but all three hyperfine levels, we generate sidebands on the 819 nm light with an electro-optical modulator. When the carrier is resonant with the $F = 11/2 \rightarrow 13/2$ transition, we obtain an increase in the loading rate of 35% with a modulation frequency of 240 MHz, i.e., when the sidebands are resonant with the two neighboring transitions. The intense and resonant output of the discharge lamp allows us to trap and detect the extremely rare isotope ^{81}Kr (9.3×10^{-13} isotopic abundance [35]) using optical excitation instead of
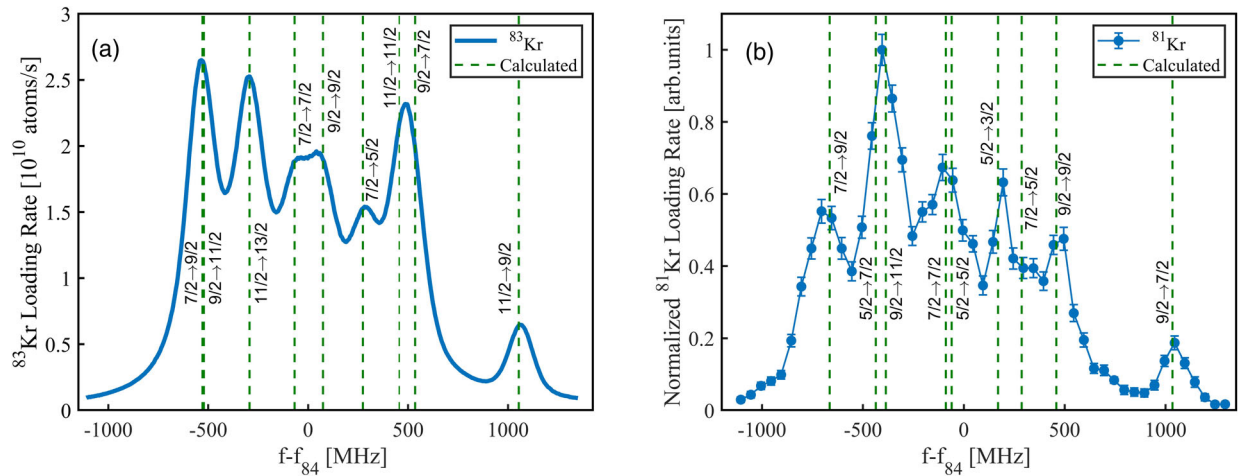

FIG. 4. (a) ^{83}Kr loading rate vs frequency of the 819 nm laser relative to the ^{84}Kr resonance. (b) ^{81}Kr loading rate vs 819 nm frequency. To cancel drifts in the trapping efficiency during the long measurement duration (3 days), the loading rate of the rare ^{81}Kr is normalized by the loading rate of the abundant ^{83}Kr (which also has hyperfine structure) measured at a fixed laser frequency. The normalized ^{81}Kr loading rate is given in arbitrary units. Its error is mainly given by the atom-counting statistics. As ^{83}Kr is abundant, its loading rate is measured with 2 MHz frequency resolution whereas the single atom loading rate of the rare ^{81}Kr is measured in steps of 50 MHz. The Doppler shifts due to the longitudinal motion of the atoms are corrected in (a) and (b) to obtain the frequency shifts at rest.
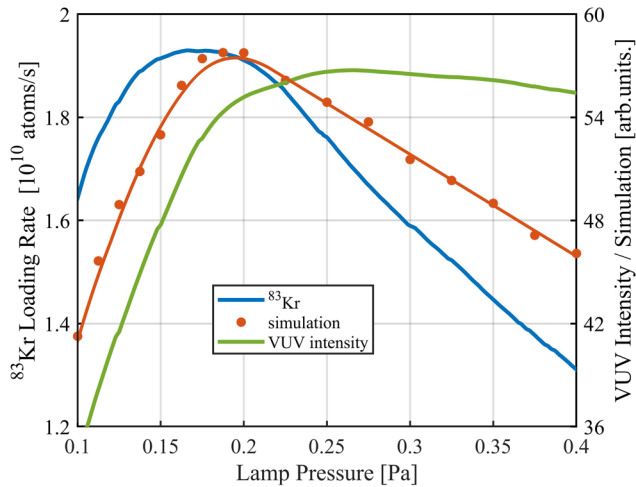
FIG. 5. ^{83}Kr loading rate, VUV intensity and simulated number of produced metastable krypton atoms vs lamp pressure. The orange line is a guide-to-the-eye for the simulated points (also orange).

TABLE I. Loading rates of the different krypton isotopes for an atmospheric krypton sample using all-optical ATTA.

Isotope	Isotopic abundance	Loading rate
^{84}Kr	57.0%	4.5×10^{11} atoms/s
^{83}Kr	11.5%	7.2×10^{10} atoms/s
^{85}Kr	1.5×10^{-11}	2.6×10^4 atoms/h
^{81}Kr	9.3×10^{-13}	1.8×10^3 atoms/h

discharge excitation. Figure 4(b) shows the normalized ^{81}Kr loading rate vs frequency of the 819 nm laser, which confirms the transition frequencies calculated in Ref. [28].

Figure 5 shows the dependence of the ^{83}Kr loading rate and the VUV intensity on the krypton pressure in the lamp. The lamp pressure (in the region on top of the window) is calculated according to the pressure measured downstream and the relevant flow conductances. At a lamp pressure of 0.2 Pa, the ^{83}Kr loading rate is ~50% higher than at 0.4 Pa, whereas the VUV intensity is almost the same. This behavior supports the result of the simulations in Fig. 3 (note the similar pressure range) that the photons are not lost at a higher lamp pressure but only become less resonant. When the lamp pressure drops below 0.2 Pa, the ^{83}Kr loading rate decreases sharply in accordance with the strongly decreasing VUV intensity. Based on the measured VUV intensity as a function of lamp pressure (Fig. 5) and the simulation of the VUV photon trajectories described above, we obtain the simulated number of produced metastables as a function of lamp pressure (Fig. 5). As the ^{83}Kr loading rate is proportional to the number of metastable atoms the two curves (blue and red) should scale together, which is indeed the case. The small difference between the optimum pressures may result because the lamp pressure close to the window region is systematically higher than the calculated value. The general agreement of the simulated and measured dependence on the lamp pressure is a further confirmation of the photon transport process described above (see also Supplemental Material [36]).

The loading rates of the odd krypton isotopes, measured using optical excitation under optimum conditions, are shown in Table I. To assess the influence of hyperfine

structure on the excitation efficiency, the loading rate of the abundant ^{84}Kr (no hyperfine structure) is also measured. The loading rate ratio between ^{84}Kr and ^{83}Kr is a little higher than their isotopic abundance ratio indicating that the sideband coverage for the odd ^{83}Kr is incomplete. The ^{83}Kr loading rate in Fig. 4 is lower than that in Table I because no sidebands on the 819 nm light were added and the transmission of the MgF$_2$ window had already decreased due to prior usage. The achieved single atom loading rates for the rare ^{81}Kr and ^{85}Kr ($t_{1/2} = 11$ a) are comparable to state-of-the-art ATTA systems based on discharge excitation [6].

The VUV intensity of the lamp presented here drops to about 50% in the first 20 h. In the following 100 h the output decreases linearly to about 30% of the initial intensity. The decrease might be caused by part of the discharge still reaching metal parts. It may thus be mitigated by making the lamp entirely with glass and the MgF$_2$ window [37,38]. Another contribution to the decreasing transmission of the MgF$_2$ window may be the formation of color centers in the MgF$_2$ crystal induced by the VUV radiation [39,40]. However, the achieved lifetime of the present lamp is already sufficient for operational use.

As described in the introduction, the conventional discharge excitation leads to sample loss and cross-sample contamination due to sputtering processes. Over a typical ^{81}Kr measurement of 4 h, about 70% of a 1 μL krypton sample is lost and ~30 nL/h of contaminant krypton is sputtered out of the system. We have measured these characteristics in our all-optical setup and find that both limitations are overcome. When filling in a 1 μL krypton sample, the loss after a 4 h measurement is below the detection limit of 5%. The krypton contamination rate is only 0.1 nL/h, 2 orders of magnitude lower than that of discharge excitation. Within measurement uncertainty the contamination rate is the same with and without lamp.

Conclusion and outlook.—With the all-optical approach we achieve a ^{81}Kr loading rate similar to state-of-the-art systems based on discharge excitation while sample loss and cross-sample contamination are negligible. Consequently, the measurement time can be extended from a few hours to a few days, gaining counting statistics accordingly. The sample size requirement of ^{81}Kr dating can thus be brought to its fundamental limit below 1 kg, with the precision given by the number of ^{81}Kr atoms

contained in a water or ice sample. These advances enable new applications for ^{81}Kr dating in the earth sciences, particularly for polar ice cores where high precision is needed and the sample size is limited. Due to the low background, all-optical ATTA can also be used to analyze sub-ppt levels of krypton in the purified xenon for the next generation of dark matter detectors [41–43]. The excitation technique realized here can readily be applied in other metastable krypton or xenon experiments. It is more demanding for metastable argon since the required VUV wavelength (107 nm) is shorter, requiring a lithium-fluoride window for sufficient transmission.

It is straightforward to further increase the optical excitation efficiency by adding more lamps. This will further reduce the measurement time for ^{81}Kr analysis and opens a new pathway for high number density metastable noble gas experiments.

---

[*]Corresponding author.
florian@ustc.edu.cn
[†]Corresponding author.
ztlu@ustc.edu.cn

[1] H. H. Loosli and H. Oeschger, Earth Planet. Sci. Lett. 7, 67 (1969).

[2] Z.-T. Lu, P. Schlosser, W. M. Smethie, N. C. Sturchio, T. P. Fischer, B. M. Kennedy, R. Purtschert, J. P. Severinghaus, D. K. Solomon, T. Tanhua, and R. Yokochi, Earth-Sci. Rev. 138, 196 (2014).

[3] C. Y. Chen, Y. M. Li, K. Bailey, T. P. O'Connor, L. Young, and Z.-T. Lu, Science 286, 1139 (1999).

[4] W. Jiang, K. Bailey, Z.-T. Lu, P. Muller, T. P. O'Connor, C.-F. Cheng, S.-M. Hu, R. Purtschert, N. C. Sturchio, Y. R. Sun, W. D. Williams, and G.-M. Yang, Geochim. Cosmochim. Acta 91, 1 (2012).

[5] L. Tian, F. Ritterbusch, J.-Q. Gu, S.-M. Hu, W. Jiang, Z.-T. Lu, D. Wang, and G.-M. Yang, Geophys. Res. Lett. 46, 6636 (2019).

[6] W. Jiang, S.-M. Hu, Z.-T. Lu, F. Ritterbusch, and G.-M. Yang, Quat. Int. 547, 166 (2020).

[7] P. U. Clark, D. Archer, D. Pollard, J. D. Blum, J. A. Rial, V. Brovkin, A. C. Mix, N. G. Pisias, and M. Roy, Quaternary Science Reviews 25, 3150 (2006).

[8] J. Severinghaus, E. W. Wolff, and E. J. Brook, Eos, Trans. Am. Geophys. Union 91, 357 (2010).

[9] J. M. Schaefer, R. C. Finkel, G. Balco, R. B. Alley, M. W. Caffee, J. P. Briner, N. E. Young, A. J. Gow, and R. Schwartz, Nature (London) 540, 252 (2016).

[10] A. M. Yau, M. L. Bender, T. Blunier, and J. Jouzel, Earth Planet. Sci. Lett. 451, 1 (2016).

[11] L. G. Thompson, T. Yao, M. E. Davis, K. A. Henderson, E. Mosley-Thompson, P.-N. Lin, J. Beer, H.-A. Synal, J. Cole-Dai, and J. F. Bolzan, Science 276, 1821 (1997).

[12] L. G. Thompson, M. E. Davis, E. Mosley-Thompson, P.-N. Lin, K. A. Henderson, and T. A. Mashiotta, J. Quat. Sci. 20, 723 (2005).

[13] S. Hou, T. M. Jenk, W. Zhang, C. Wang, S. Wu, Y. Wang, H. Pang, and M. Schwikowski, Cryosphere 12, 2341 (2018).

[14] H. A. Hyman, Phys. Rev. A 18, 441 (1978).

[15] H. A. Hyman, Phys. Rev. A 20, 855 (1979).

[16] A. A. Mityureva and V. V. Smirnov, Opt. Spectrosc. 128, 443 (2020).

[17] M. A. Dakka, G. Tsiminis, R. D. Glover, C. Perrella, J. Moffatt, N. A. Spooner, R. T. Sang, P. S. Light, and A. N. Luiten, Phys. Rev. Lett. 121, 093201 (2018).

[18] D. R. Albert, D. L. Proctor, and H. Floyd Davis, Rev. Sci. Instrum. 84, 063104 (2013).

[19] J. Wang, F. Liu, Y. Mo, Z. Wang, S. Zhang, and X. Zhang, Rev. Sci. Instrum. 88, 114102 (2017).

[20] Y. Chang, Y. Yu, H. Wang, X. Hu, Q. Li, J. Yang, S. Su, Z. He, Z. Chen, L. Che et al., Nat. Commun. 10, 1 (2019).

[21] L. Young, D. Yang, and R. W. Dunford, J. Phys. B 35, 2985 (2002).

[22] H. Daerr, M. Kohler, P. Sahling, S. Tippenhauer, A. Arabi-Hashemi, C. Becker, K. Sengstock, and M. B. Kalinowski, Rev. Sci. Instrum. 82, 073106 (2011).

[23] Y. Ding, S.-M. Hu, K. Bailey, A. M. Davis, R. W. Dunford, Z.-T. Lu, T. P. O'Connor, and L. Young, Rev. Sci. Instrum. 78, 023103 (2007).

[24] M. Kohler, H. Daerr, P. Sahling, C. Sieveke, N. Jerschabek, M. B. Kalinowski, C. Becker, and K. Sengstock, Europhys. Lett. 108, 13001 (2014).

[25] R. D. Cowan and G. H. Dieke, Rev. Mod. Phys. 20, 418 (1948).

[26] C. West and H. Human, Spectrochim. Acta B Atom. Spectros. 31, 81 (1976).

[27] Z. Weiss, J. Anal. At. Spectrom. 12, 159 (1997).

[28] Z.-Y. Zhang, F. Ritterbusch, W.-K. Hu, X.-Z. Dong, C. Y. Gao, W. Jiang, S.-Y. Liu, Z.-T. Lu, J. S. Wang, and G.-M. Yang, Phys. Rev. A 101, 053429 (2020).

[29] C. F. Cheng, G. M. Yang, W. Jiang, Y. R. Sun, L. Y. Tu, and S. M. Hu, Opt. Lett. 38, 31 (2013).

[30] H. Okabe, J. Opt. Soc. Am. 54, 478 (1964).

[31] E. Gudimenko, V. Milosavljević, and S. Daniels, Opt. Express 20, 12699 (2012).

[32] M. Goto, K. Sawada, T. Oishi, and S. Morita, J. Phys. 810, 012016 (2017).

[33] R. Kersevan and J.-L. Pons, J. Vac. Sci. Technol. A 27, 1017 (2009).

[34] O. Axner, J. Gustafsson, N. Omenetto, and J. D. Winefordner, Spectrochim. Acta B Atom. Spectros. 59, 1 (2004).

[35] J. C. Zappala, D. Baggenstos, C. Gerber, W. Jiang, B. M. Kennedy, Z.-T. Lu, J. Masarik, P. Mueller, R. Purtschert, and A. Visser, Geophys. Res. Lett. 47, e2019GL086381 (2020).

[36] See Supplemental Material at http://link.aps.org/supplemental/10.1103/PhysRevLett.127.023201 for further measurements on the photon process in the lamp and its output spectrum.

[37] G. H. C. Freeman and P. J. Moore, J. Phys. E 11, 980 (1978).

[38] I. A. Nevyazhskaya, N. V. Shilina, V. B. Shilov, and V. A. Tyapkov, J. Opt. Technol. **79**, 521 (2012).

[39] W. A. Sibley and O. E. Facey, Phys. Rev. **174**, 1076 (1968).

[40] E. V. Zhukova, V. M. Zolotarev, N. B. Margaryants, and L. P. Shishatskaya, J. Opt. Technol. **69**, 154 (2002).

[41] S. Lindemann and H. Simgen, Eur. Phys. J. C **74**, 2746 (2014).

[42] E. Aprile, D. Daw, Z. Greene, G. Plante, and T. Zhu, J. Instrum. **13**, P10018 (2018).

[43] E. Aprile *et al.* (XENON Collaboration), Nature (London) **568**, 532 (2019).